Fluid Phase Equilibria 351 (2013) 74–86

Contents lists available at SciVerse ScienceDirect

Fluid Phase Equilibria

journal homepage: www.elsevier.com/locate/fluid

High pressure CO_2 absorption studies on imidazolium-based ionic liquids: Experimental and simulation approaches

Ferdi Karadas[a], Banu Köz[b], Johan Jacquemin[c], Erhan Deniz[a], David Rooney[c], Jillian Thompson[c], Cafer T. Yavuz[d], Majeda Khraisheh[a], Santiago Aparicio[e,*], Mert Atihan[a,**]

[a] Department of Chemical Engineering, Qatar University, Doha, Qatar
[b] Department of Energy Systems Engineering Karamanoglu Mehmetbey University, Karaman, Turkey
[c] School of Chemistry and Chemical Engineering, Queen's University Belfast, Belfast, Northern Ireland, United Kingdom
[d] Graduate School of EEWS (WCU), Korea Advanced Institute of Science and Technology (KAIST), Daejeon, Republic of Korea
[e] Department of Chemistry, University of Burgos, Burgos, Spain

ARTICLE INFO

Article history:
Received 24 May 2012
Received in revised form 6 October 2012
Accepted 8 October 2012
Available online 2 November 2012

Keywords:
Ionic liquids
High-pressure
Carbon dioxide
Solubility
Imidazolium
Molecular dynamics

ABSTRACT

A combined experimental–computational study on the CO_2 absorption on 1-butyl-3-methylimidazolium hexafluophosphate, 1-ethyl-3-methylimidazolium bis[trifluoromethylsulfonyl]imide, and 1-butyl-3-methylimidazolium bis[trifluoromethylsulfonyl]imide ionic liquids is reported. The reported results allowed to infer a detailed nanoscopic vision of the absorption phenomena as a function of pressure and temperature. Absorption isotherms were measured at 318 and 338 K for pressures up to 20 MPa for ultrapure samples using a state-of-the-art magnetic suspension densimeter, for which measurement procedures are developed. A remarkable swelling effect upon CO_2 absorption was observed for pressures higher than 10 MPa, which was corrected using a method based on experimental volumetric data. The experimental data reported in this work are in good agreement with available literature isotherms. Soave–Redlich–Kwong and Peng–Robinson equations of state coupled with bi-parametric van der Waals mixing rule were used for successful correlations of experimental high pressure absorption data. Molecular dynamics results allowed to infer structural, energetic and dynamic properties of the studied CO_2 + ionic liquids mixed fluids, showing the relevant role of the strength of anion–cation interactions on fluid volumetric properties and CO_2 absorption.

1. Introduction

Ionic liquids (ILs) are salts existing in the liquid state at room temperature, consisting of large asymmetric organic cations and anions, which are resulted in low lattice energy and moderate coulombic forces [1,2]. The variability of cations and anions leading to ILs allows tailor-made ILs with desired physical and chemical properties of interest [3,4]. Most major characteristics of ILs are their low volatility and high ionic conductivity together with their good thermal and electrochemical stability [5–7], for which they have attracted academic and industrial interest [8–12] in applications such as solvents and catalysts for chemical reactions, and flue gas separation agents for chemical and other industrial processes [13,14].

Compared to traditional organic solvents, the non-volatility nature of ILs makes them benign solvents for gas treatment and separation processes [15]. ILs are reported for high solubilities of water and CO_2 compared to conventional organic solvents [16–19]. Due to solubility differences between CO_2 and other gases such as N_2, O_2, and CH_4, ILs have started to gain great academic and industrial interest for separation of CO_2 from flue gas or natural gas at pre or post combustion process streams [14,20,21]. Literature contains a large number of articles on the solubility of CO_2 in ILs [18,22–30], which show the interest, both in industry and academia, on this ILs application. Experimental studies on determining CO_2 solubilities in selected ILs have been widely investigated in recent years [27,31–40]. In particular, classic imidazolium-based ILs have been studied comprehensively for their CO_2 capture performances [41–43]. Blanchard et al. [44] reported for the very first time the properties of imidazolium-based ionic liquids as CO_2 absorbents, showing the null solubility of ionic liquids in CO_2 in comparison with the remarkable solubility of CO_2 in the ionic liquid phase. Zhang and Chan [45] reviewed the available literature on the use of imidazolium-based ionic liquids in sustainable chemistry, including CO_2 capture. Huang et al. [46] analyzed the CO_2 absorption mechanism in imidazolium-based ionic liquids from molecular dynamics simulations results through the spatial rearrangement of available free volume to accommodate CO_2 molecules but without

* Corresponding author. Tel.: +34 947 258062; fax: +34 947 258831.
** Corresponding author. Tel.: +974 4403 4142; fax: +974 4403 4131.
E-mail addresses: sapar@ubu.es (S. Aparicio), mert.atilhan@qu.edu.qa (M. Atihan).

0378-3812/$ – see front matter © 2012 Elsevier B.V. All rights reserved.
http://dx.doi.org/10.1016/j.fluid.2012.10.022

remarkable changes in anion–cation interactions. The CO_2 absorption is strongly dependent on anion type, and in a minor extension in alkyl chain lengths in imidazolium rings [46]. Brennecke and coworkers [47] analyzed the anion effect on CO_2 solubility, showing increasing absorption with anion fluorination. Nevertheless, the available results show low CO_2 capture ability for imidazolium-based ILs, i.e. up to 3.5 mol% at ambient temperature and pressure [45], which is clearly insufficient for industrial purposes, especially for flue gases treatment. Therefore, new efforts have been developed in the literature to improve CO_2 capturing ability using imidazolium-based ionic liquids. Several authors have proposed the use of amine-functionalized imidazolium-based ionic liquids, which leads to chemical absorption, and thus showing remarkable increase in CO_2 solubility but also important problems such as their very high viscosity and high energy penalties for the desorption processes [48–51].

Experimental studies have showed that the CO_2 solubility in ILs increases with pressure and decreases with temperature [39,52]. Nevertheless, most of the data available are at atmospheric or low-pressure conditions (e.g. lower than 10 MPa) [14]. The main reason for this scarcity in high pressure absorption data rises from the technical difficulties to carry out these measurements with acceptable uncertainties. High pressure data on CO_2 capture is also important to test possible sorbent materials on both pre and post combustion CO_2 capture purposes for industrial scale applications. Pre-combustion CO_2 conditions are set at higher pressures, e.g. a water–gas shift reaction produces a mixture of H_2 (61.5%) and CO_2 (35.5%) at 30 bar [53]. Pipeline compression of crude natural gas reaches [54] up to pressures in excess of 175 bar while CO_2 transport for sequestration demands [55] pressures of 150 bar. Liquefied natural gas (LNG) stack temperatures have to be limited to a maximum of 180 °C by regulations [56]. Ideally, a sorbent should tolerate all these conditions (0–175 bar and 40–180 °C), while retaining its CO_2 capacity. Most gas adsorption and absorption (sorption) experiments are measured with a volumetric, a gravimetric or combined volumetric/gravimetric equipment. There are also some other experimental techniques, which do not get serious interest due to limitations, accuracy and repeatability problems [57]. For measurements at conditions similar to process conditions the volumetric method has some limitations, because only atmospheric conditions are experimented. Recently, Rubotherm® state-of-the-art magnetic suspension sorption equipment has been used for ILs and CO_2 solubility measurements [24,58–60]. With this apparatus, measurements can be performed from 253 to 523 K for pressures up to 35 MPa, with suitable accuracy in the whole pressure–temperature ranges.

An important problem rising in the study of thermophysical behavior of ILs stands on the purity of the used samples, which has a strong effect on ILs properties [13]. Many available studies on CO_2 absorption in ILs were carried out with samples of not clarified purity. Moreover, Freire et al. [61] reported the hydrolysis of the common hexafluorophosphate and tetrafluoroborate anions, which were used in many CO_2 absorption studies paired with imidazolium-based cations. Therefore the use of ultrapure and properly characterized ILs samples is required to obtain reliable results [62].

Molecular dynamics simulations is a powerful tool to study nanoscopic behavior of complex systems such as those containing ILs + CO_2. Deschamps et al. [63] studied the CO_2 + [bmim][PF_6] system, pointing to CO_2 molecules non-interacting remarkably with C2 position in imidazolium ring and placed preferentially near the anion. Cadena et al. [29] analyzed the CO_2 + [bmim][PF_6] system showing the small volume expansion and the negligible changes in the ionic liquid structure upon CO_2 absorption. Huang et al. [46] studied the CO_2 + [bmim][PF_6] system analyzing the molecular level reasons of the low values for CO_2 partial molar volume, and showing that CO_2 molecules occupy cavities rising from small angular rearrangements of the anions without remarkable expansion. Bhargava et al. [64] studied the CO_2 + [bmim][PF_6] system showing a remarkable volume expansion and specific interaction between CO_2 molecules and $[PF_6]^-$ anions; these authors also reported that the CO_2 solvation in [bmim][PF_6] is primary controlled by the anion [65]. Kerle et al. [66] simulated the temperature dependence of CO_2 solubility in [emim][Tf_2N] and [bmim][Tf_2N], showing that the solvation free energy of CO_2 is almost insensitive to the alkyl chain length on the imidazolium cation. Shim et al. [67] studied the solvation structure of CO_2 in [bmim][PF_6] showing the appearance of preferential solvation for a diatomic probe. Yue et al. [68] carried out molecular dynamics studies of several CO_2 + imidazolium-based ionic liquids including [bmim][PF_6] and [emim][Tf_2N], showing that CO_2 molecules overlap with $[PF_6]^-$ anions around the imidazolium cation, whereas in the case of $[Tf_2N]^-$ systems no overlapping is inferred. Ghobadi et al. [69] carried out NPT Monte Carlo simulations for the CO_2 absorption in [bmim][PF_6] and [bmim][Tf_2N] ILs; the authors proposed the use of a new solubility index obtained from calculated intermolecular interaction energies to analyze gas solubility. Zhang et al. [15] published a review work recently on the use of ionic liquids for CO_2 capturing purposes in which available results from molecular modeling are also analyzed.

The enormous amount of possible anion–cation combinations leading to ILs [70] make necessary to carry out systematic studies on their properties and molecular level structure, which is especially relevant to find ILs with suitable CO_2 properties for industrial purposes between the plethora of possible candidates. This objective can be fulfilled using a combined experimental–computational approach, which on one side would provide with the required CO_2 absorption data, and on the other side would lead to the nanoscopic vision of the absorption process, and thus, allowing to obtain a vision of the relationships between sorption abilities and fluids' structuring and properties. Therefore, the results of the combined high pressure CO_2 absorption and molecular dynamics studies on three selected imidazolium-based ILs: butyl-3-methylimidazolium hexafluophosphate, [bmim][PF_6], 1-ethyl-3-methylimidazolium bis[trifluoromethylsulfonyl]imide, [emim][Tf_2N], and 1-butyl-3-methylimidazolium bis[trifluoromethylsulfonyl]imide, [bmim][Tf_2N], are reported in this work. The objectives of the work were: (*i*) to extend available information of CO_2 absorption data for imidazolium-based ionic liquids to the high pressure region using reliable and accurate state-of-the-art apparatus, (*ii*) to use samples synthesized in our laboratories, being ultrapure and well-characterized, and (*iii*) to infer molecular level information from simulation results that combined with the experimental measurements will lead to valuable information on the absorption process.

2. Materials and methods

2.1. Materials

All studied ILs were synthesized and purified in-house in the Queen's University Ionic Liquid Laboratories (QUILL) Research Centre. Prior to use, ILs were dried and degassed at pressures lower than 1 Pa for 15 h at 323.15 K whilst being stirred. After this treatment, their halide contents were determined by using Agilent® suppressed ion chromatography (IC), and lithium content of the samples prepared from the lithium salt was determined by Agilent® inductively coupled plasma analysis (ICP). Water content was determined before and after each measurement by Coulometric Karl–Fisher titration using a GR Scientific titrator. 99.99% purity CO_2 was used. Relevant properties are summarized in Table 1.

Table 1
Molar mass (M), halide mass fraction content (w_{h^-}), lithium mass fraction content (w_{Li^+}), and water content in mass fractions (w_w) of the samples used in this work.

	M (g mol^{-1})	$w_w \times 10^{-3}$	$w_{h^-} \times 10^{-6}$	$w_{Li^+} \times 10^{-6}$	Purity (mass%)
[bmim][PF_6]	284.18	0.135	<15[a]	–	
[bmim][Tf_2N]	419.37	0.055	<5[a]	0.8	
[emim][Tf_2N]	391.31	0.012	<5[a]	2.7	
CO_2	–	–	–	–	99.995

[a] Bromide mass fraction content.

2.2. Absorption measurements

High-pressure sorption isotherm data of CO_2 were collected in a magnetic suspension balance manufactured by Rubotherm® that can be operated up to 35 MPa. Details of the equipment are given elsewhere [71,72]. Pressure transducers (Paroscientific, US) were used in a range from vacuum up to 35 MPa with an accuracy of 0.01% in full scale. The temperature was kept constant with an accuracy of ±0.5 K for each measurement (Minco PRT, US). In situ density values for CO_2 are measured during sorption measurements as it is necessary to calculate the absorbed CO_2 amount, and density values are cross-checked with REFPROP 9.0 [73] for consistency purposes.

Absorption measurements were carried out using 2–3 mL samples for the corresponding IL. First the system is taken under vacuum for 24 h at 60 °C. Carbon dioxide is then pressurized via Teledyne Isco 260D fully automated gas booster and charged into the high-pressure cell, then CO_2 absorption on the sample begins. Once equilibrium is reached (~45 min), 4 different set of measurements are taken for a period of 10 min; each data point is collected at every 30 s. At the end of each pressure point, system goes, automatically, to the next pressure measurement point. In this work, pressure up to 20 MPa is used for maximum pressure, to provide full scale performance scan, and at the end of each isotherm, hysteresis check is conducted at each isotherm by collecting desorption data as the system is depressurized.

Absorption data is analyzed and the amount of adsorbed carbon dioxide on the sample is calculated by using Eq. (1):

$$W + W_{buoy,sample} + W_{buoy,sink} = m_{ads} + m_{sample} + m_{sink} \quad (1)$$

where W is the signal read by the instrument, $W_{buoy,sample} = V_{sample} \times d_{gas}$ is the buoyancy correction due to sample, V_{sample} is the volume of the sample, d_{gas} is the density of the gas, $W_{buoy,sink} = V_{sinker} \times d_{gas}$ is the buoyancy correction due to sinker, V_{sinker} is the volume of the sinker, m_{ads} is the absorption amount, m_{sample} is the mass of the sample, and m_{sink} is the mass of the sinker. The mass of empty sinker was determined at several pressures using helium to determine $W_{buoy,sink}$. V_{sinker} was calculated from the slope of weight vs. density plot obtained from this measurement. A blank measurement at vacuum was, firstly, performed to determine m_{sink}. m_{sample} is determined by performing a measurement at vacuum.

2.3. Molecular dynamics methods

Classical molecular dynamics simulations for CO_2 + ILs mixed fluids were carried out using the MDynaMix v. 5.0 molecular modeling package [74]. Simulations were performed in the NPT ensemble using the Nose–Hoover method to control the temperature and pressure of the simulation system [75]. The equations of motion were solved by Tuckerman–Berne double time step algorithm [76] with long and short time steps of 1 and 0.1 fs, respectively. The Ewald summation method [77] was implemented for the Coulombic interactions with radius cut-off of 1.5 nm. The simulated systems consist of cubic boxes of pure ionic liquids or ionic liquids with absorbed CO_2, with the compositions reported in Table S1 (Supplementary data). Simulation boxes were built using 125 ionic pairs and a number of CO_2 molecules from 14 to 125, to study composition effect on mixture properties up to equimolar systems. Initial boxes were generated placing randomly ions and CO_2 molecules in a FCC lattice at low density (~0.2 g cm^{-3}), then NPT simulations were performed at the selected pressure and temperature, equilibration was checked through constant potential energy. After equilibration, 10 ns runs (time step 1 fs) in the NPT ensemble at the studied pressure (2.5 MPa) and temperature (298 K) were performed for the analysis of systems' properties. Equimolar composition for the studied pressure and temperature are supersaturated conditions, as we may infer from experimental measurements, Table 2; nevertheless, the objective of the computational work is to analyze molecular level interaction features, not to predict phase equilibria. Force field parameterization for the studied ionic liquids were obtained from the literature [78,79], as well as those for CO_2 molecules [80].

3. Results and discussion

3.1. CO_2 absorption measurements

Sorption data from magnetic suspension apparatus is given in Fig. 1. Reported results show that for a common [bmim]$^+$ cation, CO_2 sorption increases on going from [PF_6]$^-$ to [TF_2N]$^-$ anion, and for common [TF_2N]$^-$ anion sorption increases with increasing alkyl chain length in imidazolium cation [46,47]. Nevertheless, the anion effect on sorption ability is more remarkable than the cation effect. Temperature increase lead to lower sorption abilities, as it may be expected, whereas the pressure effect seems to be more complex from Fig. 1. Although increasing pressure lead to increasing CO_2 sorption, it appears that for pressures higher than

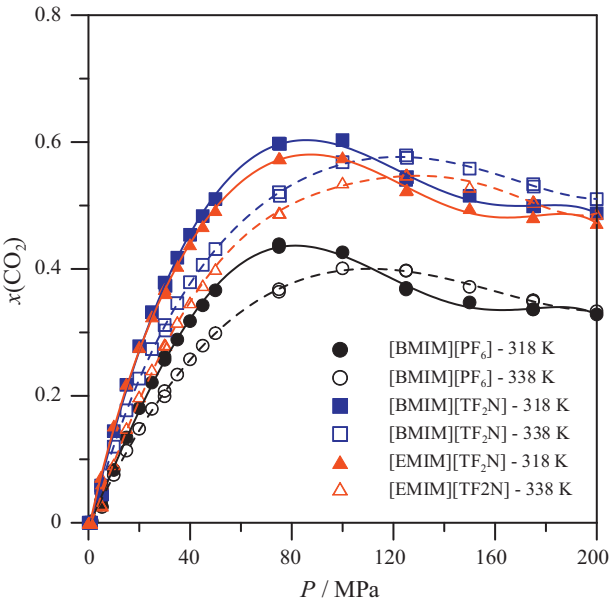

Fig. 1. Swelling uncorrected high pressure CO_2 absorption data on [bmim][PF_6], [bmim][Tf_2N] and [emim][Tf_2N].

Table 2
Experimental data of solubility of CO_2 in the studied ionic liquids, swelling corrected according to method proposed in previous section.[a]

[bmim][PF_6]				[bmim][Tf_2N]				[emim][Tf_2N]			
318 K		338 K		318 K		338 K		318 K		338 K	
P (MPa)	$x(CO_2)$	P (MPa)	$x(CO_2)$	P (MPa)	$x(CO_2)$	P (MPa)	$x(CO_2)$	P (MPa)	$x(CO_2)$	P (MPa)	$x(CO_2)$
0.0120	0.0000	0.0120	0.0000	0.0130	0.0000	0.0120	0.0000	0.0120	0.0000	0.0120	0.0000
0.0970	0.0000	0.0980	0.0006	0.1060	0.0000	0.0990	0.0000	0.0963	0.0001	0.0990	0.0000
0.4950	0.0282	0.4951	0.0346	0.5000	0.0589	0.4990	0.0550	0.4957	0.0759	0.4960	0.0326
0.9951	0.0835	0.9953	0.0761	0.9980	0.1461	0.9960	0.1211	0.9989	0.1603	1.0015	0.0990
1.4952	0.1358	1.4951	0.1153	1.4950	0.2211	1.4953	0.1800	1.4950	0.2297	1.4978	0.1597
1.9952	0.1842	1.9951	0.1509	1.9951	0.2845	1.9970	0.2322	1.9960	0.2911	1.9950	0.2128
2.4951	0.2267	2.4949	0.1839	2.4951	0.3409	2.4960	0.2810	2.4956	0.3424	2.4960	0.2588
2.9952	0.2647	2.9950	0.2137	2.9970	0.3902	2.9960	0.3213	2.9974	0.3888	2.9960	0.3015
3.4954	0.2990	3.4947	0.2416	3.4960	0.4324	3.4961	0.3583	3.4951	0.4285	3.4951	0.3400
3.9958	0.3308	3.9952	0.2677	3.9952	0.4715	3.9958	0.3941	3.9959	0.4658	3.9961	0.3741
4.4954	0.3586	4.4951	0.2916	4.4960	0.5042	4.4958	0.4243	4.4959	0.4974	4.4953	0.4044
4.9950	0.3853	4.9950	0.3137	4.9955	0.5344	4.9963	0.4522	4.9960	0.5262	4.9955	0.4333
7.4956	0.4741	7.4949	0.3976	7.4958	0.6428	7.4955	0.5583	7.4957	0.6304	7.4957	0.5403
9.9955	0.5225	9.9949	0.4518	9.9952	0.7095	9.9966	0.6288	9.9955	0.7003	9.9958	0.6132
12.4955	0.5260	12.4947	0.4812	12.4960	0.7282	12.4960	0.6768	12.4961	0.7348	12.4953	0.6670
14.9955	0.5317	14.9942	0.4924	14.9964	0.7399	14.9960	0.7008	14.9962	0.7455	14.9961	0.6977
17.4952	0.5375	17.4916	0.4966	17.4959	0.7479	17.5016	0.7119	17.4958	0.7553	17.4959	0.7139
19.9948	0.5428	19.9909	0.4997	19.9974	0.7562	19.9973	0.7149	19.9965	0.7638	19.9977	0.7226

[a] $u(T) = \pm 0.1$ K; $u(P) = \pm 0.01\%$ (full scale); $u(x) = \pm 0.0001$.

10 MPa, absorbed amounts of CO_2 on ILs show decreasing trends, which is due to the swelling effect being previously reported for high-pressure CO_2 solubility experiments in ILs, and in polymers, [81–84]. Therefore, the swelling-uncorrected data reported in Fig. 1 should be corrected considering the swelling effect rising upon CO_2 absorption, for which several procedures are possible.

3.2. Correction of swelling effect on sorption data

Swelling phenomena needs correction for determining absolute CO_2 capture performance at elevated pressures [22–24,81]. Most reported experimental sorption data have been obtained at low or moderate pressures, where the CO_2 solubility is relatively low and the IL swelling can be neglected. Uncorrected CO_2 high pressure sorption data at elevated pressures, Fig. 1, are analyzed considering Eq. (2).

$$\Delta m = m_A + m_s + m_{SK} - W_{SK} - W_{S\text{-}A} \quad (2)$$

where Δm stands for the experimental readings, m_A for the mass of absorbed gas (CO_2), m_S for the IL mass, m_{SK} for the sinker mass, W_{SK} for the buoyancy correction due to sinker, and $W_{S\text{-}A}$ for the combined buoyancy correction due to ionic liquid and absorbed gas. Buoyancy corrections are calculated according to Eqs. (3) and (4):

$$W_{SK} = V_{SK} d_G \quad (3)$$

$$W_{S\text{-}A} = \left(\frac{m_S + m_A}{d_{S\text{-}A}}\right) d_G = V_{S\text{-}A} d_G \quad (4)$$

where V_{SK} stands for the sinker volume, $d_{S\text{-}A}$ and $V_{S\text{-}A}$ for density and volume, respectively, of IL sample with absorbed gas. The buoyancy effect due to IL sample and absorbed gas, $W_{S\text{-}A}$, changes with the amount of absorbed gas due to the swelling effect, with increasing amounts of absorbed gas the fluid expands leading to larger $V_{S\text{-}A}$ values and to larger $W_{S\text{-}A}$ contributions. As m_A increases with pressure for isothermal conditions, $W_{S\text{-}A}$ will be more important for the high-pressure region whereas it is almost negligible in the low-pressure region. Rearranging Eqs. (2) and (5) is obtained:

$$m_A = \Delta m - m_S - m_{SK} + W_{SK} + W_{S\text{-}A} \quad (5)$$

The third first terms in Eq. (5) are experimental amounts:

$$C = \Delta m - m_S - m_{SK} \quad (6)$$

The problem rises into the calculation of $W_{S\text{-}A}$ through the determination of exact values of $V_{S\text{-}A}$. In this work, experimental swelling data for the studied systems coming from the literature is used to calculate the $V_{S\text{-}A}$ term. Aki et al. [47] reported CO_2 absorption and volumetric data for [bmim][PF_6] and [bmim][Tf_2N] ionic liquids. Ren et al. [85] reported data for [emim][Tf_2N]. Aki et al. [47] reported data at 313.15 and 333.15 K for [bmim][PF_6] and [bmim][Tf_2N], and Ren et al. [85] at 323.15 and 343.15 K for [emim][Tf_2N], whereas experimental measurements were carried out at 318 and 338 K in this work. Nevertheless, molar volume is reported in Fig. 2, V_m, as a function of CO_2 mole fraction for the two temperatures close to measurements reported in this work, showing that V_m does not change for the studied temperature range for the three considered ILs. Therefore, experimental V_m data coming from the literature [47,85] is used, from which, experimental m_S were recalculated, and thus, $V_{S\text{-}A}$ is obtained as a function of m_A, Fig. 3. These values do not change within the studied temperature range, and thus, they were fitted together (temperature independent) according to a linear model for each IL, Eq. (7):

$$V_{S\text{-}A} = a_1 m_A + a_0 \quad (7)$$

Combining Eqs. (5)–(7), Eq. (8) is obtained:

$$m_A = C + W_{SK} + (a_1 m_A + a_0) d_G \quad (8)$$

Eq. (8) was solved for each experimental point leading to swelling corrected CO_2 absorption data, Table 2 and Fig. 4. Swelling corrected data were compared with those available into the literature, Figs. S1–S5 (Supplementary data). The main differences rise for [bmim][PF_6], Fig. S1 (Supplementary data); deviations with Aki et al. [47] and Liu et al. [86] are more than the comparisons to those reported by Zhang et al. [87], Shiflett and Yokozeki [88], Kumelan et al. [89], and Kamps et al. [90]. Aki et al. [47] reported the strong effect of decomposition products from the degradation of $[PF_6]^-$ anion on the CO_2 solubility measurements, which could justify the differences between the data reported in this work and those reported in some literature sources, although it should be remarked the excellent agreement between data reported in this work and other literature sources. Data for [bmim][Tf_2N] and [emim][Tf_2N] are in excellent agreement with literature values [38,47,85,91,92,31,93], Figs. S2 and S3 (Supplementary data).

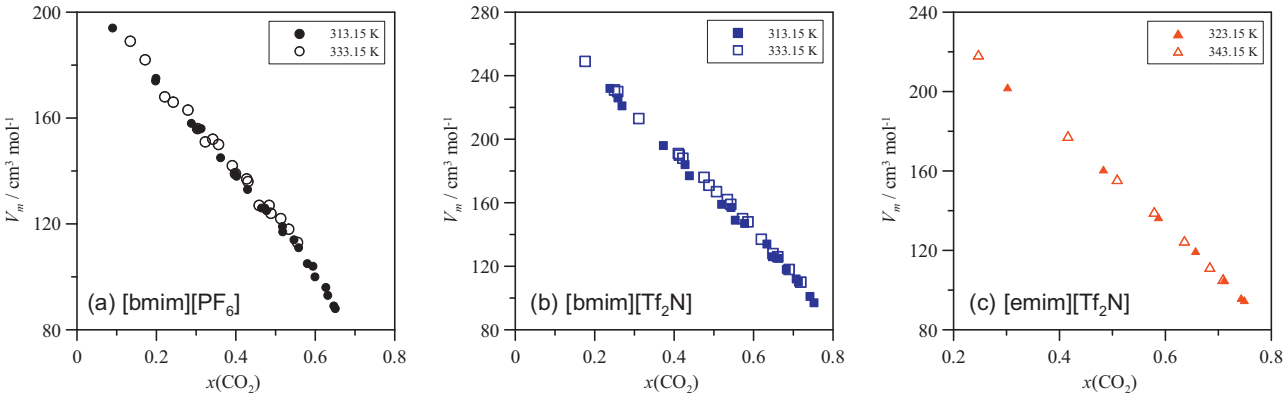

Fig. 2. Variation of molar volume, V_m, with the mole fraction of absorbed CO_2.
Experimental data from Aki et al. [47] and Ren et al. [85].

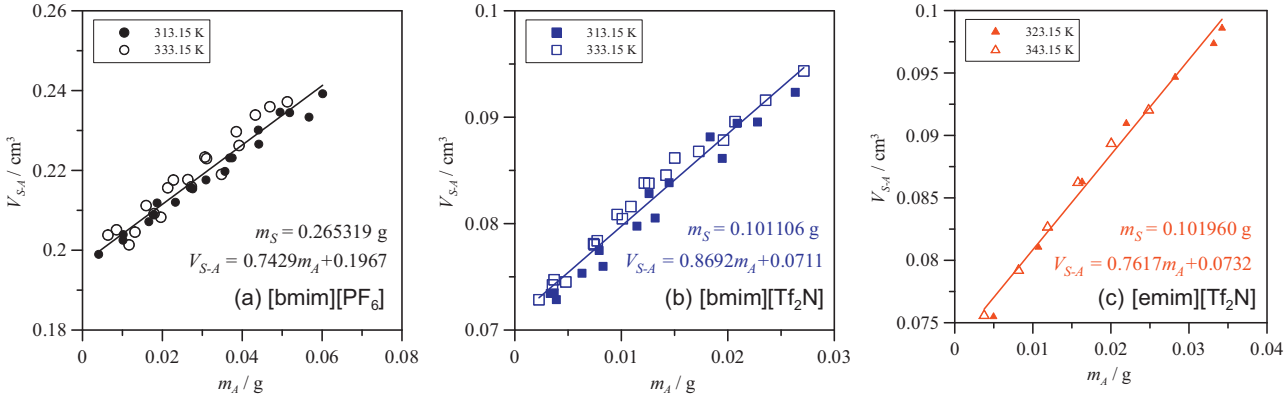

Fig. 3. Variation of sample volume (swelling), V_{S-A}, with the amount of absorbed CO_2 (m_A).

3.3. Correlation of absorption data using cubic equations of state

Experimental CO_2 absorption data (vapor–liquid equilibrium data) were correlated using Peng–Robinson (PR) and Soave–Redlich–Kwong (SRK) equations of state (EOS), combined with van der Waals 2-parameter mixing rule [94]. Critical properties and acentric factors required for EOS calculations, Table 3, were obtained from Valderrama and Robles [95] who used a group contribution method to predict these properties. Correlation results are reported in Table 4 and Fig. 5, both EOS lead to satisfactory

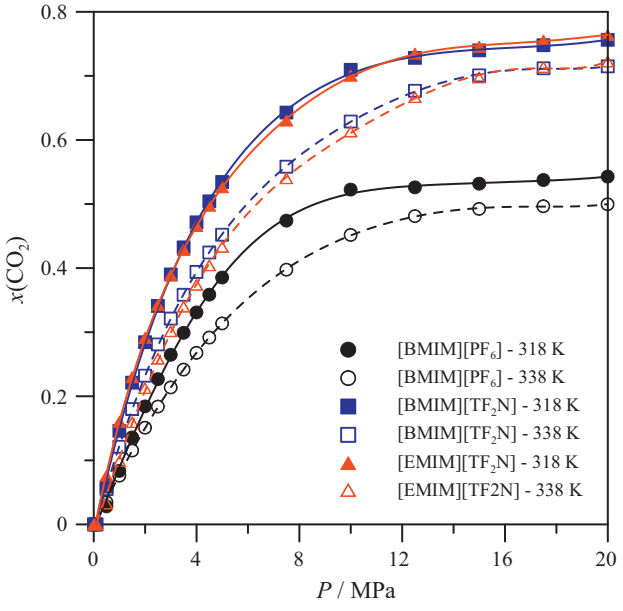

Fig. 4. Isothermal experimental solubility data of CO_2 in the studied ionic liquids. $x(CO_2)$ stands for CO_2 mole fraction.

Table 3
Critical properties and acentric factors used for EOS calculations.

	T_c (K)	P_c (MPa)	V_c (cm^3 mol^{-1})	w
[bmim][PF$_6$][a]	708.9	1.73	779.5	0.7553
[bmim][Tf$_2$N][a]	1265.0	2.76	1007.1	0.2656
[emim][Tf$_2$N][a]	1244.9	3.26	892.9	0.1818
CO_2 [b]	304.13	7.38	94.1	0.2239

[a] Data from Valderrama and Robles [95].
[b] Data from REFPROP 9.0 [73].

Table 4
Binary interaction parameters (k_{12} and l_{12}) and equations of state correlation results for ionic liquid + CO_2 vapor liquid equilibria. *%AARD* stands for percentage absolute average relative deviation.

	T (K)	PR			SRK		
		k_{12}	l_{12}	*%AARD*	k_{12}	l_{12}	*%AARD*
[bmim][PF$_6$]	318	0.2096	0.0400	1.57	0.2134	0.0394	1.49
	338	0.2491	0.0536	1.00	0.2528	0.0462	0.91
[emim][Tf$_2$N]	318	0.0547	0.0267	1.73	0.0555	0.0270	1.77
	338	0.0508	0.0294	1.43	0.0555	0.0317	1.49
[emim][Tf$_2$N]	318	0.0536	0.0330	1.11	0.0523	0.0332	1.15
	338	0.0440	0.0251	1.56	0.0446	0.0281	1.62

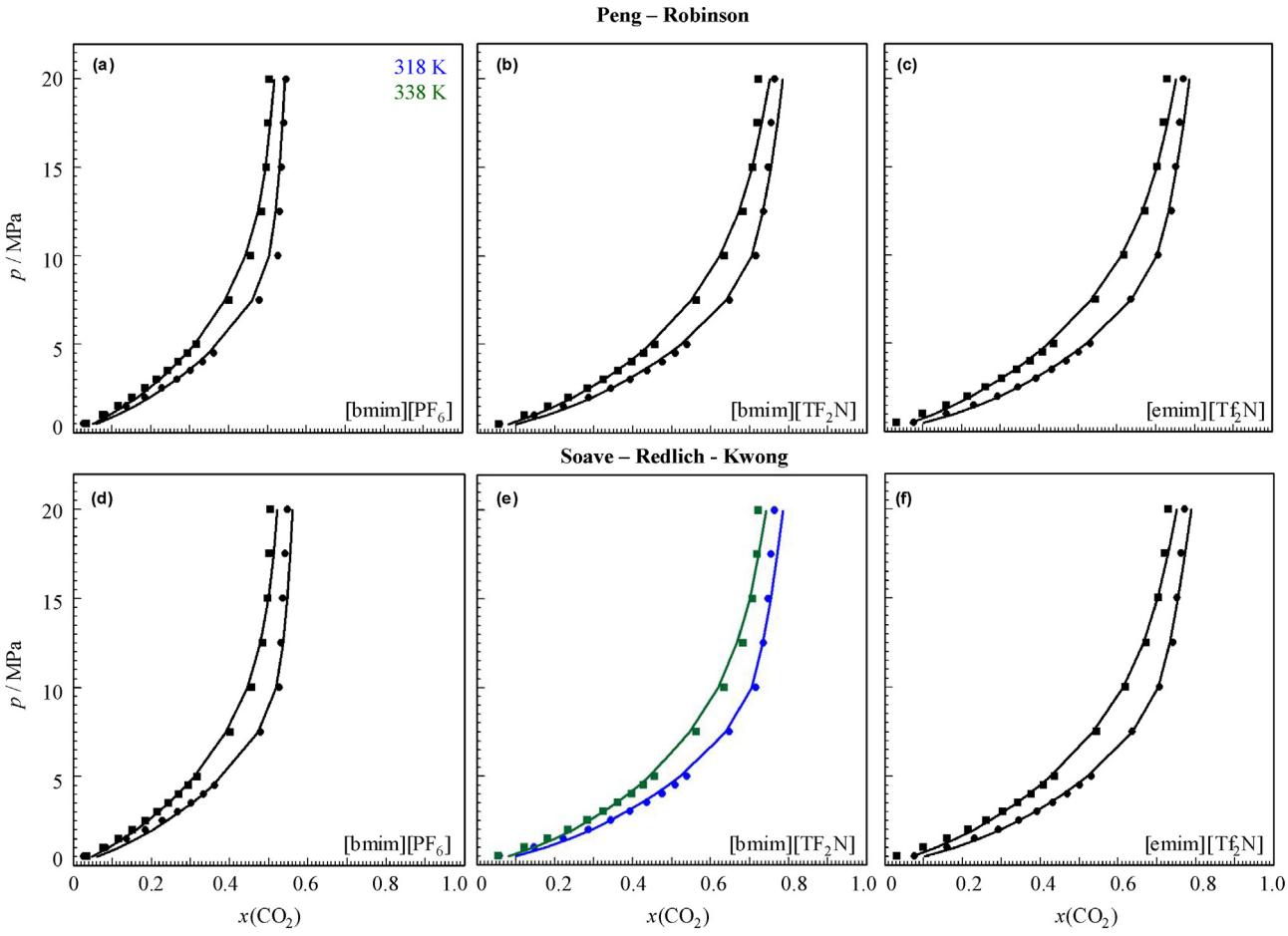

Fig. 5. Results of CO_2 absorption data correlation using Peng–Robinson and Soave–Redlich–Kwong equations of state with binary interaction parameters reported in Table 2.

correlation, with percentage absolute average relative deviation lower than 1.77% for both fluids and EOS.

Ren et al. [85] reported the appearance of vapor–liquid–liquid equilibrium and liquid–liquid equilibrium for [emim][Tf_2N] + CO_2 system at 298.15 K. High-pressure phase diagrams for [emim][Tf_2N] + CO_2 system were extrapolated using the binary interaction parameters reported in Table 4, for 318 and 338 K, which are reported in Fig. 6 in comparison with that reported by Ren et al. [85] at 298.15 K. The results reported in Fig. 6 show mixture critical points, which some authors have discarded for CO_2 + ionic liquid systems [26,85] by considering it as an artifact of the EOS predictions in the high pressure regions. The results reported in Fig. 6 for 318 and 338 K do not show the existence neither of three phase lines (vapor–liquid–liquid equilibria), nor of liquid–liquid equilibria because they are above the critical point of pure CO_2.

3.4. Molecular dynamics

Simulations were carried out as a function of absorbed CO_2 mole fraction (from pure ionic liquids to CO_2 equimolar systems, Table S1, Supplementary data) for the three studied ionic liquids ([emim][Tf_2N], [bmim][Tf_2N] and [bmim][PF_6]). The analysis of molecular dynamics results reported in this work will be done considering: (*i*) structural microscopic features, using radial distribution functions (RDFs) and spatial distribution functions (SDFs), together with volume expansion upon CO_2 absorption (swelling effect) (*ii*) energetic features, using intermolecular interaction energies, and (*iii*) dynamic properties, using self-diffusion coefficients. Detailed center of mass RDFs, and their corresponding coordination numbers, are reported in Figs. S4–S9, Supplementary data. The main conclusion that may be inferred from the evolution of RDFs with increasing CO_2 mole fraction is

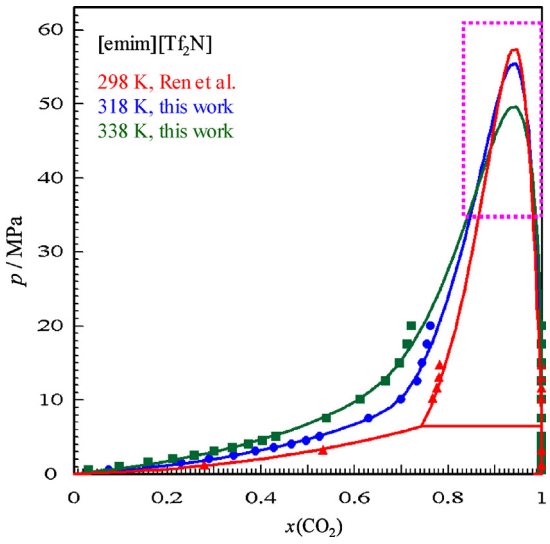

Fig. 6. Phase equilibria for [emim][Tf_2N] + CO_2. Lines show Peng–Robinson correlation results with parameters reported in Table 2, circles show experimental data. Data at 298 K obtained from Ren et al. [85]. Dashed pink lines show the Peng–Robinson predictions of mixture critical points. (For interpretation of the references to color in this figure legend, the reader is referred to the web version of the article.)

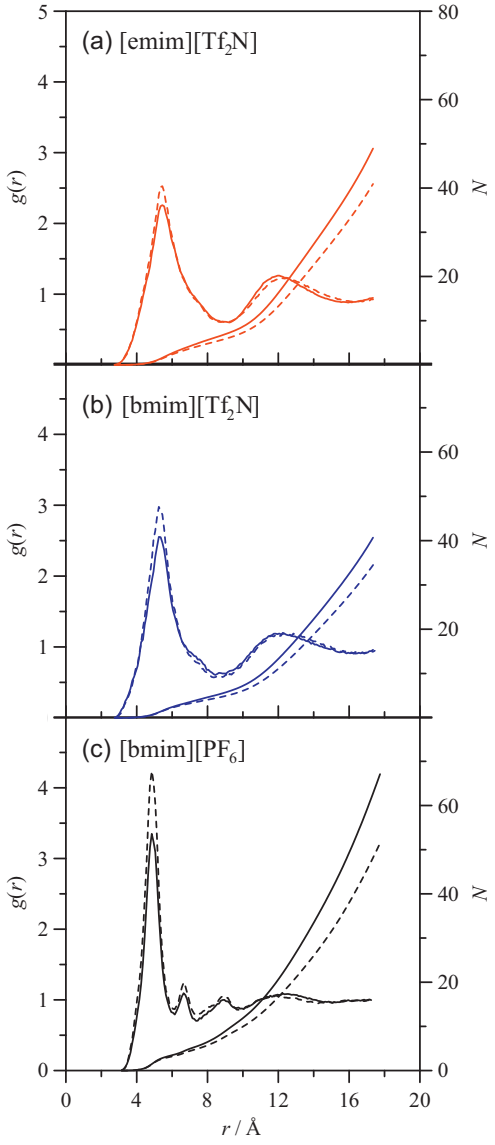

Fig. 7. Anion–cation center-of-mass radial distribution functions, $g(r)$, and the corresponding coordination numbers, N, for $x\mathrm{CO_2}+(1-x)$ {(a) [emim][$\mathrm{Tf_2N}$] or (b) [bmim][$\mathrm{Tf_2N}$] or (c) [bmim][$\mathrm{PF_6}$]} systems, at 298 K and 2.5 MPa obtained from molecular dynamics simulations. Continuous lines correspond to $x = 0$ (pure ionic liquids) and dashed lines to $x = 0.5$ systems.

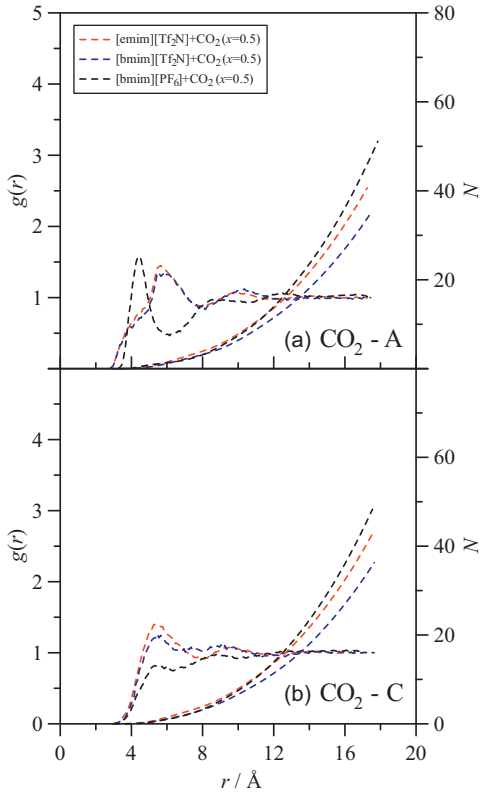

Fig. 8. (a) $\mathrm{CO_2}$–anion and (b) $\mathrm{CO_2}$–cation center-of-mass radial distribution functions, $g(r)$, and the corresponding coordination numbers, N, for $x\,(=0.5)\,\mathrm{CO_2}+(1-x)$ {[emim][$\mathrm{Tf_2N}$] or [bmim][$\mathrm{Tf_2N}$] or [bmim][$\mathrm{PF_6}$]} systems, at 298 K and 2.5 MPa obtained from molecular dynamics simulations. A stands for anion, and C for cation.

the absence of remarkable changes in the ion–ion interactions, Figs. S4, S6, and S8 (panels a–c, Supplementary data). Only very subtle changes are inferred for anion–cation RDFs, as shown in Fig. 7, leading to a decrease in the coordination number. Nevertheless this decrease is almost negligible in the first solvation shell (~8 Å) for the three studied ionic liquids, and thus short and medium range anion–cation interactions are not affected by the presence of $\mathrm{CO_2}$ molecules when considering concentrations as high as equimolar solutions. $\mathrm{CO_2}$–ion RDFs are reported in Fig. 8, the structuring of $\mathrm{CO_2}$ is different around anion and cation, and also remarkable differences are inferred when considering $[\mathrm{PF_6}]^-$ and $[\mathrm{Tf_2N}]^-$ anions. Kanakubo et al. [96] reported a X-ray diffraction study of [bmim][$\mathrm{PF_6}$] + $\mathrm{CO_2}$ mixtures showing $\mathrm{CO_2}$ molecules preferentially solvating the $[\mathrm{PF_6}]^-$ anion. This preferential solvation is confirmed by the RDFs reported in Fig. 8 [29,64,65]. Nevertheless, for [$\mathrm{Tf_2N}$] containing systems, the differences of $\mathrm{CO_2}$ distributions around anion and cation are more subtle. A more detailed picture of the spatial distribution of the involved molecules may be obtained from SDFs reported in Figs. 9 and 10 and Fig. S10 (Supplementary data), which show SDFs for {[emim][$\mathrm{Tf_2N}$] or [bmim][$\mathrm{Tf_2N}$]} + $\mathrm{CO_2}$ systems being clearly different to those for [bmim][$\mathrm{PF_6}$] + $\mathrm{CO_2}$. SDFs around imidazolium cations show that they interact with $[\mathrm{Tf_2N}]^-$ anion preferentially through the region opposite to the fluorine atoms, without remarkable changes between pure ionic liquids and equimolar $\mathrm{CO_2}$ solutions, Figs. 9 and 10 and Fig. S10 (Supplementary data, panels a and b). For [bmim][$\mathrm{PF_6}$] systems, imidazolium cations solvate $[\mathrm{PF_6}]^-$ anions in the well-known octahedral distribution because of its spherical symmetry and charge distribution [65]. Nevertheless, anion distribution around imidazolium cations is very similar both for $[\mathrm{Tf_2N}]^-$ and $[\mathrm{PF_6}]^-$, Figs. 9 and 10 and Fig. S10 (Supplementary data, panels d and e). The distribution of $\mathrm{CO_2}$ around anions is remarkable different for $[\mathrm{Tf_2N}]^-$ and $[\mathrm{PF_6}]^-$ ions, Figs. 9 and 10 and Fig. S10 (Supplementary data, panel c), and also different for the distribution around cations (Figs. 9 and 10 and Fig. S10, Supplementary data, panel f). Therefore the presence of spherical $[\mathrm{PF_6}]^-$ anion leads to remarkable changes in the molecular structuring and $\mathrm{CO_2}$ distribution in the studied ionic liquids.

The structural differences rising from the presence of $[\mathrm{PF_6}]^-$ anion in comparison with $[\mathrm{Tf_2N}]^-$ should justify the different $\mathrm{CO_2}$ solubility (lower for $[\mathrm{PF_6}]^-$ based systems). Several studies have analyzed the relationship of available free space in ionic liquids with gas solubility, and the ionic liquid volume expansion upon $\mathrm{CO_2}$ absorption. Huang et al. [46] carried out simulation studies to analyze the small partial molar volume of $\mathrm{CO_2}$ in [bmim][$\mathrm{PF_6}$], which was justified through the spatial rearrangement of cavities in the ionic liquid. The most relevant volumetric properties for the three studied systems are reported in Fig. 11. Molar volume follows a linear increase with increasing $\mathrm{CO_2}$ mole fraction, with slopes increasing with increasing alkyl chain length on the cation for a fixed anion ($[\mathrm{Tf_2N}]^-$), and with lower slopes for $[\mathrm{PF_6}]^-$ containing

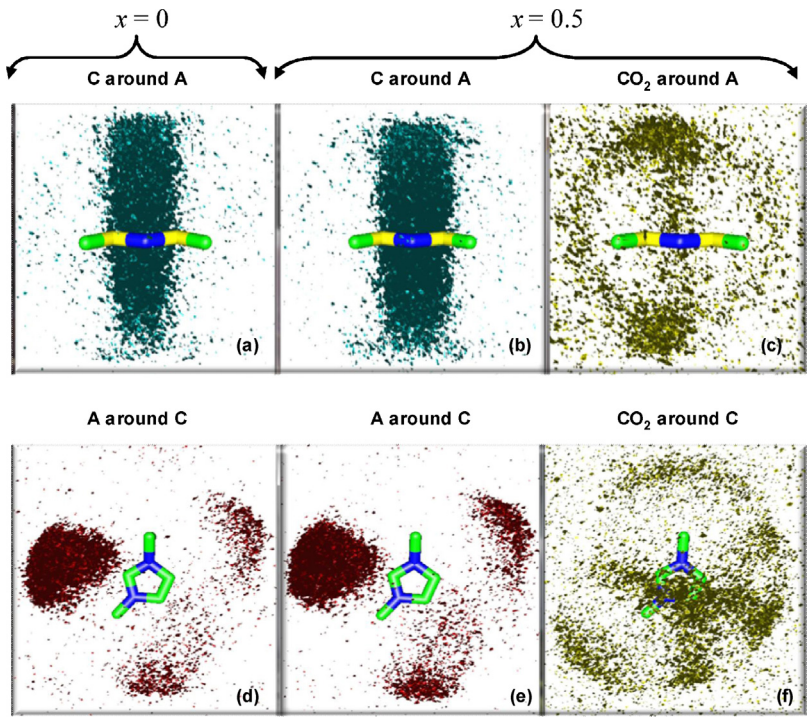

Fig. 9. Spatial distribution functions in $xCO_2 + (1-x)$ [emim][Tf_2N] systems as a function of composition, at 298 K and 2.5 MPa obtained from molecular dynamics simulations. In panels a–d blue and red surfaces show 7 times average bulk density, and in panels c and f yellow surfaces show 6 times average bulk density. A stands for anion and C for cation. (For interpretation of the references to color in this figure legend, the reader is referred to the web version of the article.)

systems, Fig. 11a. Percentage volume expansion, $\%V_{expansion}$, is defined as the change in absolute volume of the ionic liquid [47], eq. (9):

$$\%V_{expansion} = 100 \times \frac{V_{mix}(T,P,x) - V_{IL}(T,P_0)}{V_{IL}(T,P_0)} \quad (9)$$

where subindices mix and IL stand for the volume of IL + CO_2 and IL systems, respectively. $\%V_{expansion}$ reported in Fig. 11c is larger than values obtained from experimental data [47]. Aki et al. [47] reported a percentage volume expansion of 16.8% and 14.2% at 298.15 K and equimolar composition, for [bmim][PF_6] and [bmim][Tf_2N], respectively, whereas data calculated in this work are 31% and 17.9%, respectively. The main differences appear for [bmim][PF_6], which could rise from the used samples for experimental measurements, as previously mentioned, and in the forcefield parameterization used in this work. Bhargava et al. [64] also obtained slightly larger expansions for CO_2 + [bmim][PF_6] system using molecular dynamics simulations. Nevertheless, the trends are in agreement with experimental data: (*i*) lower expansions for larger imidazolium

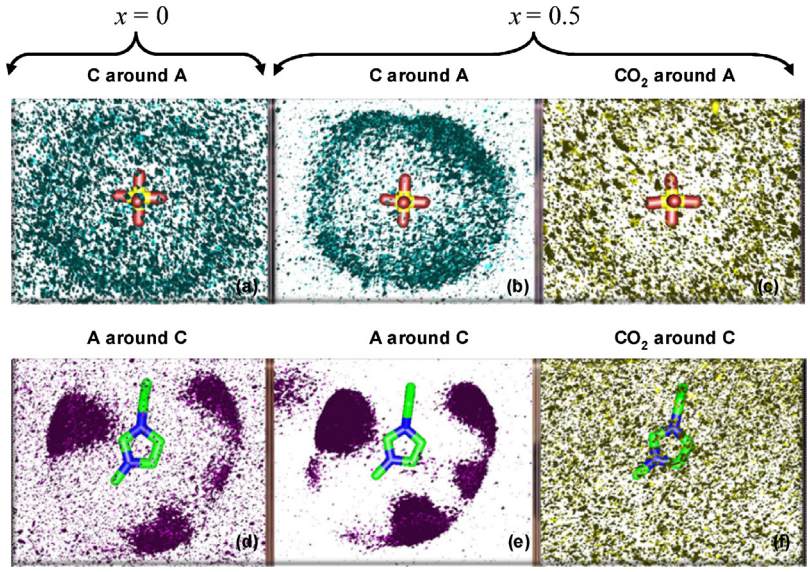

Fig. 10. Spatial distribution functions in $xCO_2 + (1-x)$ [bmim][PF_6] systems as a function of composition, at 298 K and 2.5 MPa obtained from molecular dynamics simulations. In panels a–d blue and red surfaces show 7 times average bulk density, and in panels c and f yellow surfaces show 6 times average bulk density. A stands for anion and C for cation. (For interpretation of the references to color in this figure legend, the reader is referred to the web version of the article.)

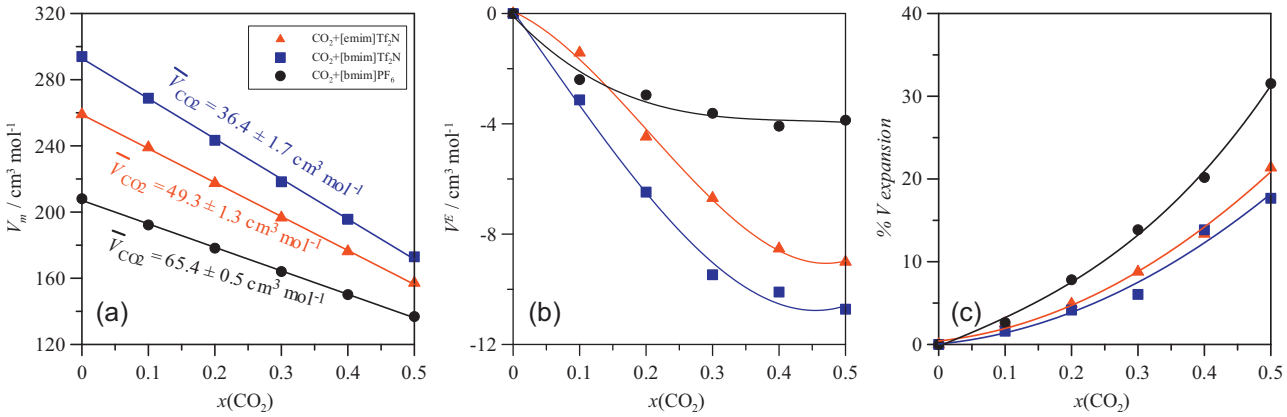

Fig. 11. (a) Molar volume, V_m, (b) excess molar volume, V^E, and (c) liquid phase volume expansion upon CO_2 absorption, $\%V_{expansion}$, for $xCO_2 + (1-x)$ {[emim][Tf_2N] or [bmim][Tf_2N] or [bmim][PF_6]} systems, at 298 K and 2.5 MPa obtained from molecular dynamics simulations. In panel (a) lines show linear fits, and in panels (b and c) lines show polynomial fits, for guiding purposes. In panel (a) we report calculated CO_2 partial molar volume.

alkyl chain for a fixed anion and (*ii*) larger expansion for $[PF_6]^-$ containing systems. Excess molar volume, calculated from simulated data using the method previously proposed [97], shows large negative values (up to $-10.7\,cm^3\,mol^{-1}$ for [bmim][Tf_2N], Fig. 11b), which is in agreement with the low expansion upon CO_2 absorption and with the absorption mechanism proposed by Huang et al. [46].

Intermolecular interaction energies are analyzed in Figs. 12 and 13 and Fig. S11 (Supplementary data). The energy of the studied systems is calculated in this work using the forcefield expression reported in Eq. (10):

$$E = \sum_{\text{bonds}} k_r(r - r_{eq})^2 + \sum_{\text{angles}} k_\theta(\theta - \theta_{eq})^2 + E_{tor} + \sum_i \sum_j \left\{ 4\varepsilon_{ij} \left[\left(\frac{\sigma_{ij}}{r_{ij}}\right)^{12} - \left(\frac{\sigma_{ij}}{r_{ij}}\right)^{6} \right] + \frac{q_i q_j e^2}{4\pi\varepsilon_0 r_{ij}} \right\} \quad (10)$$

where the first three terms correspond to bonds, angles and dihedral contribution, and the last two terms to intermolecular

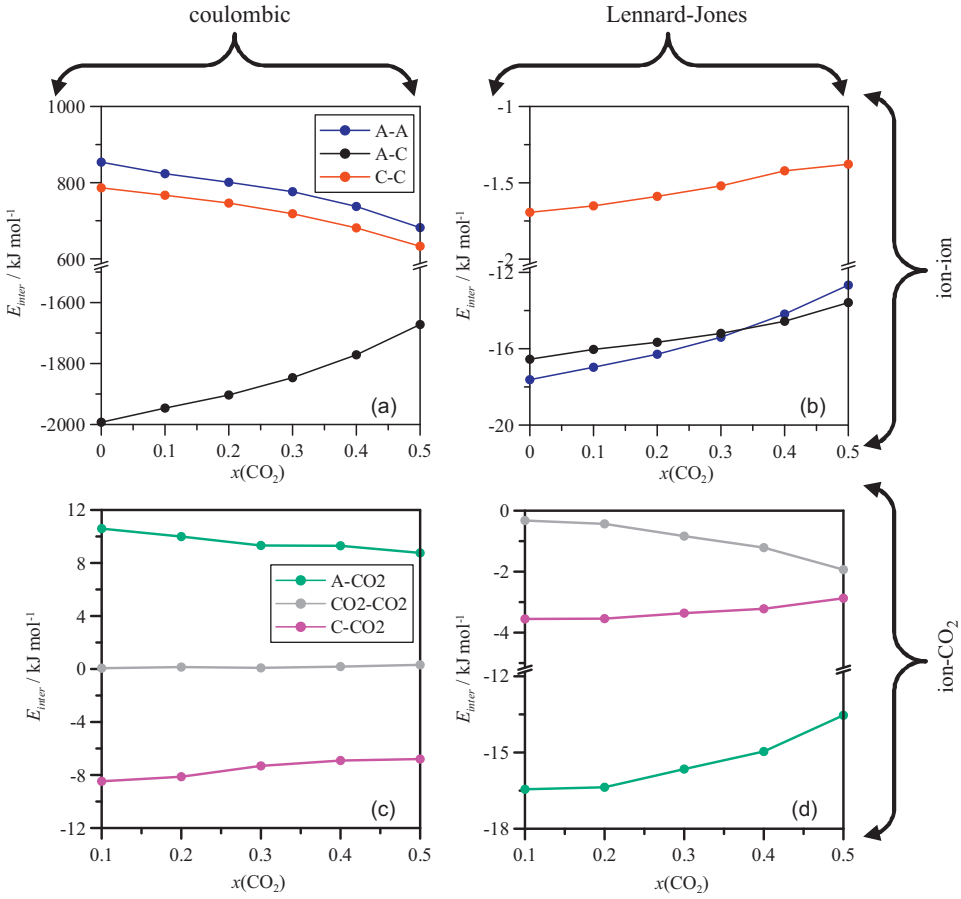

Fig. 12. Split of intermolecular interaction energies in the liquid phase of xCO_2 + [emim][Tf_2N] at 298 K and 2.5 MPa obtained from molecular dynamics simulations.

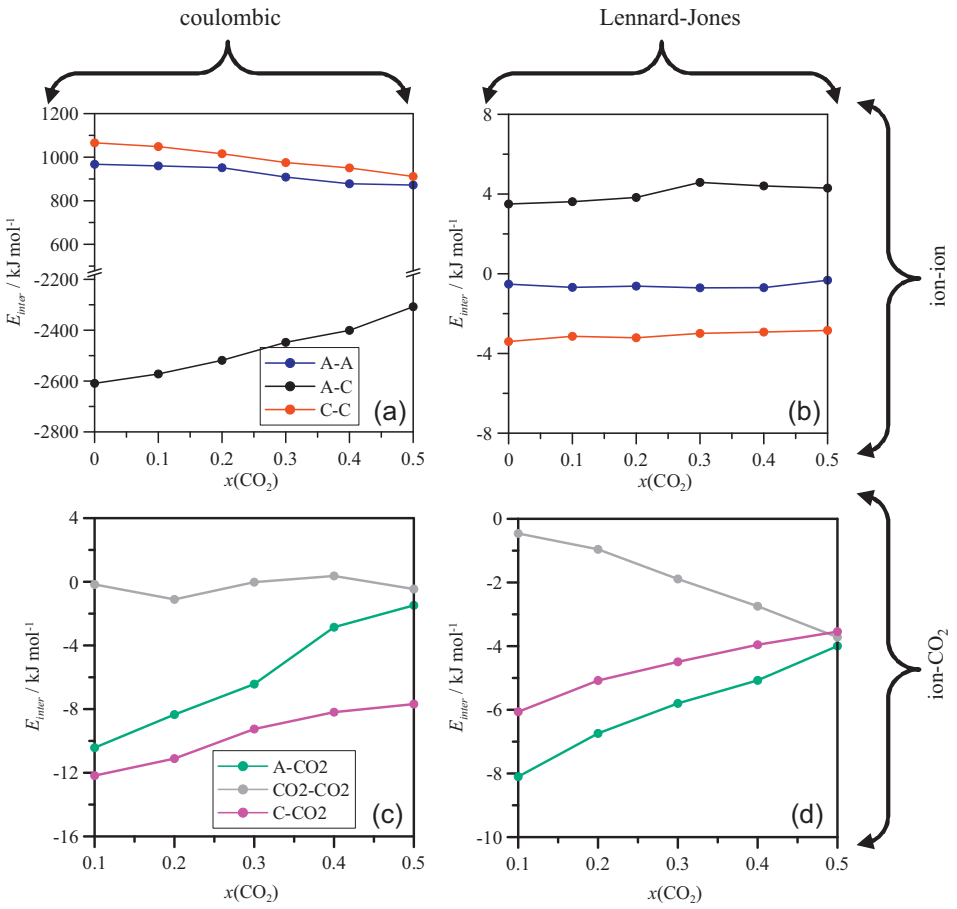

Fig. 13. Split of intermolecular interaction energies in the liquid phase of xCO_2 + [bmim][PF_6] at 298 K and 2.5 MPa obtained from molecular dynamics simulations.

energies, which are split in Lennard–Jones and coulombic contributions. For [emim][Tf_2N] and [bmim][Tf_2N] systems, intermolecular energies are very similar, Fig. 12 and Fig. S11 (Supplementary data, panels a and b), although by increasing the alkyl chain length on imidazolium cation, energy for ion–ion interactions decreases (in absolute value). For example, for pure ionic liquids coulombic anion–cation energy decrease in a 15% caused the presence of a larger alkyl chain, which leads to a certain degree of steric hindrance weakening anion–cation interaction. With increasing CO_2 concentration anion–cation coulombic interaction energy interaction decreases (in absolute value) in an almost linear way (15% and 12% for [emim][Tf_2N] and [bmim][Tf_2N], respectively). Variations in Lennard–Jones contributions for ion–ion interactions are almost negligible with increasing CO_2 mole fraction. CO_2–anion and CO_2–cation coulombic contributions show almost the same values but with opposite signs, whereas the Lennard–Jones contributions are larger for the interactions with the $[Tf_2N]^-$ anion, but CO_2–cation interactions are also important. For the [bmim][PF_6] ionic liquid, Fig. 13, ion–ion interaction energies are larger than for [bmim][Tf_2N], for example in pure ionic liquids anion–cation interaction energies are 53% larger (in absolute value) in [bmim][PF_6], an cation–cation interactions are also 54% larger. Ion–ion interaction energies decreases linearly with increasing CO_2 amounts for [bmim][PF_6], i.e. anion–cation energy decreases a 8% on going from pure ionic liquid to equimolar CO_2 solutions, Fig. 13a, which is half of the decreasing for [emim][Tf_2N] and [bmim][Tf_2N] systems. Therefore, the larger anion–cation interaction energies for [bmim][PF_6] systems are related with the lower CO_2 solubility in this ionic liquid, the absorbed CO_2 is not able to weaken it as effectively as for $[Tf_2N]^-$ containing systems. Therefore, this behavior together with the larger expansion volume in [bmim][PF_6] (fitting CO_2 molecules requires more cavities changes) would justify the effect of $[PF_6]^-$ anion on CO_2 solubility in [bmim][PF_6] in comparison with $[Tf_2N]^-$-based ILs. Furthermore, from an energetic viewpoint the interaction of CO_2 with ions in [bmim][PF_6] is also different to those calculated in $[Tf_2N]^-$ systems, showing stronger ion–CO_2 coulombic and Lennard–Jones interactions in the case of the [bmim][PF_6], Fig. 13 (panels c and d). Nevertheless, although ion–CO_2 interactions are stronger for [bmim][PF_6], which should be a factor to increase CO_2 solubility in comparison with $[Tf_2N]^-$ systems, the differences are not very remarkable, and thus the main effects controlling absorption rise from the ability of ionic liquid to fit CO_2 molecules (poorer in $[PF_6]^-$ containing systems, therefore a factor lowering solubility) and the ability of CO_2 molecules to disrupt ionic liquid structuring (also poorer in $[PF_6]^-$ based systems).

Self-diffusion coefficients, D, were calculated using the Einstein relationship. The reliability of calculated D values was inferred from the β parameter [98,99], which should be $\beta = 1$ for fully diffusive regime. [emim][Tf_2N] and [bmim][Tf_2N] are moderately viscous fluids (34.1 and 51.0 mPa s, for [emim][Tf_2N] [100] and [bmim][Tf_2N] [102], respectively at 298.15 K and 0.1 MPa), whereas viscosity for [bmim][PF_6] is remarkably larger (270.9 mPa s at 298.15 K and 0.1 MPa) [101]. Therefore, fully diffusive regime would be reached for shorter simulation times in [emim][Tf_2N] and [bmim][Tf_2N] than in [bmim][PF_6]. Nevertheless, the length of the simulations allows reaching fully diffusive regime, and thus, for [emim][Tf_2N] and [bmim][Tf_2N] systems a value of $\beta > 0.99$ was used for D calculations and $\beta > 0.95$ in the case of [bmim][PF_6] systems. The results reported in Fig. 14 show larger D values for cations than for anions, which is in agreement with

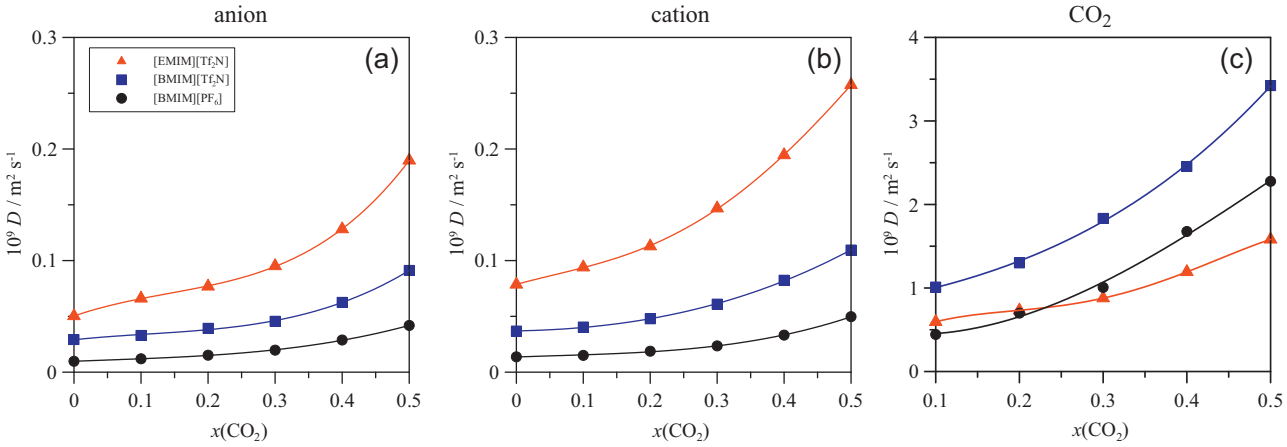

Fig. 14. Self-diffusion coefficients, D, for (a) anion, (b) cation and (c) CO_2 in $xCO_2 + (1-x)$ {[emim][Tf_2N] or [bmim][Tf_2N] or [bmim][PF_6]} systems, at 298 K and 2.5 MPa obtained from molecular dynamics simulations. Lines show polynomial fits for guiding purposes.

experimental measurements reported into the literature [102,103], and D values for CO_2 molecules are an order of magnitude larger than those for the corresponding ions. Ion D values follow the ordering [emim][Tf_2N] > [bmim][Tf_2N] > [bmim][PF_6], which is in agreement with the viscosity values and also with the interaction energies reported in Figs. 12 and 13 and Fig. S11 (Supplementary data). CO_2 absorption leads to a non-linear increase of ion D values with increasing mole fraction: (*i*) up to $x(CO_2) \sim 0.3$ weak variations are inferred and (*ii*) for $x(CO_2) > 0.3$ a steepest increase is obtained; Fig. 14 (panels a and b). Therefore, the faster the ionic diffusion, the larger the CO_2 solubility, although the effect of absorbed CO_2 on ionic diffusion is only remarkable for larger CO_2 mole fractions. D values for CO_2 molecules increase with increasing mole fraction with the larger values obtained for [bmim][Tf_2N].

4. Conclusions

High-pressure absorption measurements of CO_2 in selected classical imidazolium-based ionic liquids were carried out using new state-of-the-art apparatus up to 20 MPa. A remarkable swelling effect upon CO_2 absorption was observed from pressures higher than 10 MPa, which leaded to an apparent decrease of the CO_2 absorbed amount. A method based on the use of available experimental volumetric data for the CO_2 + ionic liquid systems is used to correct swelling effect. The corrected results are in good agreement with most of the available literature experimental data.

High-pressure absorption data were successfully correlated using Soave–Redlich–Kwong and Peng–Robinson equations of state coupled with bi-parametric van der Waals mixing rule. The obtained binary interaction parameters lead to the appearance of mixture critical points, which is not in agreement with the available literature information.

Classical molecular dynamics simulations were used to analyze the nanoscopic structural behavior of CO_2 + ionic liquids mixed systems as a function of mixture composition. The reported results show the different structuring of CO_2 around anions and cations, with the most important effect of anion type on CO_2 absorption. The anion effect is explained considering the larger expansion upon CO_2 absorption for $[PF_6]^-$ containing systems. From the viewpoint of intermolecular interaction energies, anion–cation interaction energies are remarkably for [bmim][PF_6] in comparison with $[Tf_2N]^-$ containing systems, which leaded to lower CO_2 absorption abilities for $[PF_6]^-$ containing systems. The analysis of mixtures' dynamic properties showed a direct relationship between ionic diffusion and CO_2 solubility.

The results reported in this work show the remarkable information, both form macro and microscopic viewpoints, that may inferred from high pressure absorption measurements coupled with molecular simulations

List of symbols

[bmim][PF_6] 1-butyl-3-methylimidazolium hexafluophosphate
[emim][Tf_2N] 1-ethyl-3-methylimidazolium bis[trifluoromethylsulfonyl]imide
[bmim][Tf_2N] 1-butyl-3-methylimidazolium bis[trifluoromethylsulfonyl]imide
EOS equation of state
IL ionic liquid
PR Peng–Robinson equation of state
RDF radial distribution function
SDF spatial distribution function
SRK Soave–Redlich–Kwong equation of state
%AARD percentage absolute average relative deviation
D self-diffusion coefficient
d_{gas} bensity of the gas, Eq. (1)
$d_{S\text{-}A}$ density of IL sample plus absorbed gas, Eq. (2)
Δm experimental readings, Eq. (2)
k_{12} and l_{12} binary interaction parameters
m_{ads} adsorption amount, Eq. (1)
m_A mass of absorbed gas, Eq. (2)
m_S mass of ionic liquid, Eq. (2)
m_{sample} mass of the sample, Eq. (1)
m_{sink} mass of the sinker, Eq. (1)
m_{SK} mass of sinker, Eq. (2)
N coordination numbers from RDFs
V_m molar volume, V_{sample} volume of the sample, Eq. (1)
$V_{S\text{-}A}$ volume of IL sample plus absorbed gas, Eq. (2)
V_{sinker} volume of the sinker, Eq. (1)
$W_{buoy,sample}$ buoyancy correction due to sample, Eq. (1)
$W_{buoy,sink}$ buoyancy correction due to sinker, Eq. (1)
W_{SK} buoyancy correction due to sinker, Eq. (2)
$W_{S\text{-}A}$ combined buoyancy correction due to ionic liquid and absorbed gas, Eq. (2)

Acknowledgements

This publication was made possible by NPRP grant # [09-739-2-284] from the Qatar National Research Fund (a member of Qatar

Foundation). The statements made herein are solely the responsibility of the authors.

Appendix A. Supplementary data

Supplementary data associated with this article can be found, in the online version, at http://dx.doi.org/10.1016/j.fluid.2012.10.022.

References

[1] P. Scovazzo, D. Camper, J. Kieft, J. Poshusta, C. Koval, R. Noble, Ind. Eng. Chem. Res. 43 (2004) 6855–6860.
[2] J.G. Huddleston, A.E. Visser, W.M. Reichert, H.D. Willauer, G.A. Broker, R.D. Rogers, Green Chem. 3 (2003) 156–164.
[3] J.N.A. Canongia Lopes, A.A.H. Padua, J. Phys. Chem. B 110 (2006) 3330–3335.
[4] A.A.H. Padua, M.F. Costa Gomes, J.N.A. Canongia Lopes, Acc. Chem. Res. 40 (40) (2007) 1087–1096.
[5] D. Kerle, R. Ludwig, A. Geiger, D. Paschek, J.Phys. Chem. B 113 (2009) 12727–12735.
[6] X. Han, D.W. Armstrong, Acc. Chem. Res. 40 (2007) 1079–1086.
[7] L.P.N. Rebelo, J.N.A. Canongia Lopes, J.M.S.S. Esperanca, H.J.R. Guedes, J. Lachwa, V. Najdanovic-Visak, Z.P. Visak, Acc. Chem. Res. 40 (2007) 1114–1121.
[8] Ionic Liquids From Knowledge to Application, vol. 132, American Chemical Society, 2010.
[9] M. Freemantle, Chem. Eng. News 78 (2000) 37–50.
[10] M. Freemantle, Chem. Eng. News 82 (2004) 44–49.
[11] R. Renner, Environ. Sci. Technol. 35 (2001) 410A–413A.
[12] D. Rochefort, J. Am. Chem. Soc. 131 (2009), 17031-17031.
[13] S. Aparicio, M. Atilhan, F. Karadas, Ind. Eng. Chem. Res. 49 (2010) 9580–9595.
[14] F. Karadas, M. Atilhan, S. Aparicio, Energy Fuel 24 (2010) 5817–5828.
[15] J. Zhang, J. Sun, X. Zhang, Y. Zhao, S. Zhang, Greenhouse Gas Sci. Technol. 1 (2011) 142–159.
[16] J.L. Anthony, J.M. Crosthwaite, D.G. Hert, S.N.V.K. Aki, E.J. Maginn, J.F. Brennecke, Phase equilibria of gases and liquids with 1-butyl-3-methylimidazolium tetrafluoroborate Ionic Liquids as Green Solvents, vol. 856, American Chemical Society, 2003, p. 110.
[17] J.L. Anthony, E.J. Maginn, J.F. Brennecke, Gas solubilities in 1-butyl-3-methylimidazolium hexafluorophosphate Ionic Liquids, vol. 818, American Chemical Society, 2002, p. 260.
[18] J.L. Anthony, E.J. Maginn, J.F. Brennecke, J. Phys. Chem. B 106 (2002) 7315–7320.
[19] A.M. Scurto, S.N.V.K. Aki, J.F. Brennecke, J. Am. Chem. Soc. 124 (2002) 10276–10277.
[20] J.F. Brennecke, B.E. Gurkan, J. Phys. Chem. Lett. 1 (2010) 3459–3464.
[21] M. Ramdin, T.W. de Loos, T.J.H. Vlugt, Ind. Eng. Chem. Res. 51 (2012) 8149–8177.
[22] A. Blasig, J. Tang, X. Hu, Y. Shen, M. Radosz, Fluid Phase Equilibr. 256 (2007) 75–80.
[23] A. Blasig, J. Tang, X. Hu, S.P. Tan, Y. Shen, M. Radosz, Ind. Eng. Chem. Res. 46 (2007) 5542–5547.
[24] T. Fieback, F. Dreisbach, M. Petermann, R. Span, E. Weidner, Fluid Phase Equilibr. 301 (2011) 217–224.
[25] J. Kumełan, A. Pérez-Salado Kamps, D. Tuma, G. Maurer, J. Chem. Thermodyn. 38 (2006) 1396–1401.
[26] L.A. Blanchard, Z. Gu, J.F. Brennecke, J. Phys. Chem. B 105 (2001) 2437–2444.
[27] Y.S. Kim, W.Y. Choi, J.H. Jang, K.P. Yoo, C.S. Lee, Fluid Phase Equilibr. 228–229 (2005) 439–445.
[28] J.L. Anthony, J.L. Anderson, E.J. Maginn, J.F. Brennecke, J. Phys. Chem. B 109 (2005) 6366–6374.
[29] C. Cadena, J.L. Anthony, J.K. Shah, T.I. Morrow, J.F. Brennecke, E.J. Maginn, J. Am. Chem. Soc. 126 (2004) 5300–5308.
[30] X. Zhang, Z. Xhang, H. Dong, Z. Zhao, S. Zhang, Y. Huang, Energy Environ. Sci. 5 (2012) 6668–6681.
[31] P.J. Carvalho, V.H. Alvarez, J.J.B. Machado, J. Pauly, J.L. Daridon, I.M. Marrucho, M. Aznar, J.A.P. Coutinho, J. Supercrit. Fluid 48 (2009) 99–107.
[32] P.J. Carvalho, V.H. Alvarez, I.M. Marrucho, M. Aznar, J.A.P. Coutinho, J. Supercrit. Fluid 52 (2010) 258–265.
[33] J. Jacquemin, M.F. Costa Gomes, P. Husson, V. Majer, J. Chem. Thermodyn. 38 (2006) 490–502.
[34] J.E. Kim, J.S. Lim, J.W. Kang, Fluid Phase Equilibr. 306 (2011) 251–255.
[35] J. Kumelan, A. Perez-Salado Kamps, D. Tuma, G. Maurer, J. Chem. Thermodyn. 38 (2006) 1396–1401.
[36] J. Kumelan, A. Perez-Salado Kamps, D. Tuma, G. Maurer, Fluid Phase Equilibr. 260 (2007) 3–8.
[37] C. Myers, H. Pennline, D. Luebke, J. Ilconich, J.K. Dixon, E.J. Maginn, J.F. Brennecke, J. Membr. Sci. 322 (2008) 28–31.
[38] A.M. Schilderman, S. Raeissi, C.J. Peters, Fluid Phase Equilibr. 260 (2007) 19–22.
[39] A.N. Soriano, B.T. Doma Jr., M.H. Li, J. Taiwan Inst. Chem. Eng. 40 (2009) 387–393.
[40] A.N. Soriano, B.T. Doma Jr., M.H. Li, J. Chem. Thermodyn. 41 (2009) 525–529.
[41] S.N. Baker, G.A. Baker, M.A. Kane, F.V. Bright, J. Phys. Chem. B (2001) 9663–9668.
[42] Q. Zhou, L.S. Wang, H.P. Chen, J. Chem. Eng. Data 51 (2006) 905–908.
[43] H.C. Chang, J.C. Jiang, C.Y. Chang, J.C. Su, C.H. Hung, Y.C. Liou, S.H. Lin, J. Phys. Chem. B 112 (2008) 4351–4356.
[44] L.A. Blanchard, D. Hancu, E.J. Beckman, J.F. Brennecke, Nature 399 (1999) 28–29.
[45] Y. Zhang, J.Y.G. Chan, Energy Environ. Sci. 3 (2010) 408–417.
[46] X. Huang, C.J. Margulis, Y. Li, B.J. Berne, J. Am. Chem. Soc. 125 (2005) 17842–17851.
[47] S.N.V.K. Aki, B.R. Mellein, E.M. Saurer, J.F. Brennecke, J. Phys. Chem. B 108 (2004) 20355–20365.
[48] E.D. Bates, R.D. Mayton, I. Ntai, J.H.J. Davis, J. Am. Chem. Soc. 124 (2002) 926–927.
[49] X. Li, M. Hou, Z. Zhang, B. Han, G. Yang, X. Wang, L. Zou, Green Chem. 10 (2008) 879–884.
[50] L.M. Galan, Sanchez, G.W. Meindersma, A.B. Haan, Chem. Eng. Res. Des. 85 (2007) 31–39.
[51] P. Sharma, S.D. Park, K.T. Park, S.C. Nam, S.K. Jeong, Y. Yoon, I.H. Baek, Chem. Eng. J. 193–194 (2012) 267–275.
[52] J. Palomar, M. Gonzalez, A. Polo, F. Rodriguez, Ind. Eng. Chem. Res. 50 (2011) 3452–3463.
[53] D.M. D'Alessandro, B. Smit, J.R. Long, Angew. Chem. Int. Ed. 49 (2010) 6058–6082.
[54] S. Mokhatab, W.A. Poe, M.J. Economides, World Oil 227 (2006) 113.
[55] G.T. Rochelle, Science 325 (2009) 1652–1654.
[56] A.J. Kidnay, W.R. Parrish, Fundamentals of Natural Gas Processing, CRC Press, 2006.
[57] Y. Belmabkhout, Meas. Sci. Technol. 15 (2004) 848–858.
[58] J. Lu, F. Yan, J. Texter, Prog. Polym. Sci. 34 (2009) 431–448.
[59] M. Petermann, T. Weissert, S. Kareth, H.W. Losch, F. Dreisbach, J. Supercrit. Fluid 45 (2008) 156–160.
[60] N.M. Yunus, M.I. Abdul, Z. Man, M.A. Bustam, T. Murugesan, Chem. Eng. J. 189–190 (2012) 94–100.
[61] M.G. Freire, C.M.S.S. Neves, I.M. Marrucho, J.A.P. Coutinho, A.M. Fernandes, J. Phys. Chem. A 114 (2010) 3744–3749.
[62] K.N. Marsh, J.F. Brennecke, R.D. Chirico, M. Frenkel, A. Heintz, J.W. Magee, C.J. Peters, L.P.N. Rebelo, K.R. Seddon, Pure Appl. Chem. 81 (2009) 781–790.
[63] J. Deschamps, M.F. Costa Gomes, A.A.H. Padua, ChemPhysChem 5 (2004) 1049–1052.
[64] B.L. Bhargava, A.C. Krishna, S. Balasubramanian, J. AIChE 54 (2008) 2971–2980.
[65] B.L. Bhargava, S. Balasubramanian, J. Phys. Chem. B 111 (2007) 4477–4487.
[66] D. Kerle, R. Ludwig, A. Geiger, D. Paschek, J. Phys. Chem. B 113 (2009) 12727–12735.
[67] Y. Shim, H.J. Kim, J. Phys. Chem. B 114 (2010) 10160–10170.
[68] Z.G. Yue, X.M. Liu, Y.L. Zhao, X.C. Zhang, X.M. Lu, S.J. Zhang, Chinese J. Proc. Eng. 11 (2011) 652–659.
[69] A.F. Ghobadi, V. Taghikhani, J.R. Elliott, J. Phys. Chem. B 115 (2011) 13599–13607.
[70] J.D. Holbrey, K.R. Seddon, Clean Technol. Environ. Policy 1 (1999) 223–236.
[71] S. Zulfiqar, F. Karadas, J. Park, E. Deniz, G.D. Stucky, Y. Jung, M. Atilhan, C.T. Yavuz, Energy Environ. Sci. 4 (2011) 4528–4531.
[72] F. Karadas, C.T. Yavuz, S. Zulfiqar, S. Aparicio, G.D. Stucky, M. Atilhan, Langmuir 27 (2011) 10642–10647.
[73] E.W. Lemmon, M.L. Huber, M.O. McLinden, NIST Standard Reference Database 23: Reference Fluid Thermodynamic and Transport Properties-REFPROP, Version 9.0, National Institute of Standards and Technology, Standard Reference Data Program, Gaithersburg, MD, 2010.
[74] A.P. Lyubartsev, A. Laaksonen, Comput. Phys. Commun. 128 (2000) 565–589.
[75] W.G. Hoover, Phys. Rev. A 31 (1985) 1695–1697.
[76] M. Tuckerman, B.J. Berne, G.J. Martyna, J. Chem. Phys. 97 (1992) 1990–2001.
[77] U. Essmann, L. Perera, M.L. Berkowitz, T. Darden, L. Hsing, L.G. Pedersen, J. Chem. Phys. 103 (1995) 8577–8593.
[78] T.I. Morrow, E.J. Maginn, J. Phys. Chem. B 106 (2002) 12807–12813.
[79] N.Y. Van-Oanh, C. Houriez, B. Rousseau, Phys. Chem. Chem. Phys. 12 (2010) 930–936.
[80] W. Shi, E.J. Maginn, J. Phys. Chem. B 112 (2008) 2045–2055.
[81] T.M. Fieback, F. Dreisbach, Ind. Eng. Chem. Res. 50 (2011) 7049–7055.
[82] A. Rajendran, B. Bonavoglia, N. Forrer, G. Storti, M. Mazzotti, M. Morbidelli, Ind. Eng. Chem. Res. 44 (2004) 2549–2560.
[83] I. Sakellarios Nikolaos, Ionic Liquids III A: Fundamentals, Progress, Challenges, and Opportunities, vol. 901, American Chemical Society, 2005.
[84] I. Sakellarios Nikolaos, G. Kazarian Sergei, In situ IR spectroscopic study of the CO_2 induced swelling of ionic liquid media Ionic Liquids III A: Fundamentals, Progress, Challenges, and Opportunities, vol. 901, American Chemical Society, 2005, p. 89.
[85] W. Ren, B. Sensenich, A.M. Scurto, J. Chem. Thermodyn. 42 (2010) 305–311.
[86] Z. Liu, W. Wu, B. Han, Z. Dong, G. Zhao, J. Wang, T. Jiang, G. Yang, Chem. Eur. J. 9 (2003) 3897–3903.
[87] S. Zhang, X. Yuan, Y. Chen, X. Zhang, J. Chem. Eng. Data 50 (2005) 1582–1585.
[88] M.B. Shiflett, A. Yokozeki, Ind. Eng. Chem. Res. 44 (2005) 4453–4464.
[89] J. Kumelan, A. Perez-Salado Kamps, D. Tuma, G. Maurer, J. Chem. Eng. Data 51 (2006) 1802–1807.
[90] A.P.S. Kamps, D. Tuma, J. Xia, G. Maurer, J. Chem. Eng. Data 48 (2003) 746–749.
[91] S. Raeissi, C.J. Peters, J. Chem. Eng. Data 54 (2009) 382–386.
[92] B.C. Lee, S.L. Outcalt, J. Chem. Eng. Data 51 (2006) 892–897.
[93] A. Shariati, C.J. Peters, J. Supercrit. Fluid 34 (2005) 171–176.

[94] H. Orbey, S. Sandler, Modeling Vapor–Liquid Equilibria: Cubic Equations of State and their Mixing Rules, Cambridge University Press, Cambridge, 1998.
[95] J.O. Valderrama, P.A. Robles, Ind. Eng. Chem. Res. 46 (2007) 1338–1344.
[96] M. Kanakubo, T. Umecky, Y. Hiejima, T. Aizawa, H. Nanjo, Y. Kameda, J. Phys. Chem. B 109 (2005) 13847–13850.
[97] S. Aparicio, M. Atilhan, M. Khraisheh, R. Alcalde, J. Fernandez, J. Phys. Chem. B 115 (2011) 12487–12498.
[98] S. Aparicio, M. Atilhan, M. Khraisheh, R. Alcalde, J. Phys. Chem. B 115 (2011) 12473–12486.
[99] M.G. Del Popolo, G.A. Voth, J. Phys. Chem. B 108 (2004) 1744–1752.
[100] A. Ahosseini, A.M. Scurto, Int. J. Thermophys. 29 (2008) 1222–1243.
[101] K.R. Harris, M. Kanakubo, L.A. Woolf, J. Chem. Eng. Data 52 (2007) 1080–1085.
[102] H. Tokuda, K. Hayamizu, K. Ishii, M.A.B.H. Susan, M. Watanabe, J. Phys. Chem. B 108 (2004) 16593–16600.
[103] H. Tokuda, K. Hayamizu, K. Ishii, M.A.B.H. Susan, M. Watanabe, J. Phys. Chem. B 109 (2005) 6103–6110.